Journal of Materials Chemistry A

Accepted Manuscript

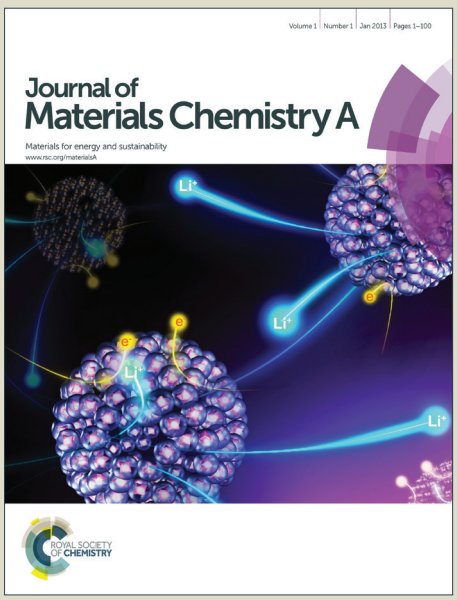

ROYAL SOCIETY OF CHEMISTRY

www.rsc.org/materialsA

Journal of Materials Chemistry A RSCPublishing

COMMUNICATION

Alkylated Phase Change Composites for Thermal Energy Storage Based on Surface-Modified Silica Aerogels

Cite this: DOI: 10.1039/xoxxoooooox

Received ooth January 2012,
Accepted ooth January 2012

DOI: 10.1039/xoxxoooooox

www.rsc.org/

Xinyu Huang‡, Zhenpu Liu‡, Wei Xia, Ruqiang Zou* and Ray P. S. Han*

We alkylated silica aerogels to make them hydrophobic for an effective impregnation and storage of a phase change material (PCM). As a result of this surface modification treatment, the aerogel scaffold exhibited an average increase of 20.9-34.7% in the PCM uptake with an improved thermal energy storage capacity and stability. For the light to thermal energy conversion experiments, we carbonized the treated aerogels and observed that they readily attained temperatures above the melting point of the PCM. Therefore, the carbonized PCM- impregnated scaffold possesses enhanced thermal energy storage and release property via a phase change response in the encapsulated PCM.

With increasing energy consumption from solar irradiation and its demand for energy efficiency, thermal energy storage has become the focus of attention.[1-7] Of the various thermal energy storage methods, the latent heat storage of PCMs is considered as having tremendous potential due to its high energy storage density and thermal energy storage at a constant to near constant temperature associated with the phase transition temperature.[8-13] Organic solid-liquid PCMs possess the merits of a wide transition temperature range, a high latent heat storage capacity, no or low supercooling and good chemical and thermal stability.[14-18] However, many conventional PCMs cannot be applied directly; they need to be recombined with an appropriate base material to overcome their inherent defects, which include volumetric changes during the phase change process and leakages in the melted state.

Impregnation in a porous material is an effective way to hold a PCM and prevent its leakages during the phase transition.[19-25] By adjusting and/or selecting the pore size of the scaffold, their capillary force can be suitably tuned to maximize the PCM encapsulation.[26-28] Chen et al.[29] reported a phase change composite based on paraffin wax-infiltrated carbon nanotube sponge, which made use of the high porosity and oil-wetting surface in the carbon nanotube sponge. Paraffin wax was confined in the pores of carbon nanotube sponge by capillary forces and intermolecular C-H•••π interaction, and the phase change composite showed good thermal cycling performance without leakage from the melting paraffin during the phase change processes. However, the scaffold material generally, has very little contribution to the thermal storage, and thus, its weight should be kept to a minimum.

Silica (SiO_2) aerogel is a synthetic ultralight material with a very high pore volume and a large internal surface area,[30-32] but the hydroxyl ends in the microstructure limit its potential for storage capability, especially for impregnation by an organic PCM.[33] Zhou et al. [34] worked on a SiO_2 aerogel infiltrated with a solid-liquid PCM, erythritol. However, the resulting composite is hydrophilic with a hydroxyl end group and the structure is unstable as it can collapse in a humid atmosphere. Since most organic PCMs with long carbon chains are hydrophobic, they cannot effectively wet Zhou's hydrophilic porous aerogel, and this in turn, will adversely impact the PCM impregnation. Additionally, a supercritical fluid is required to dry the SiO_2 aerogel with an autoclave needed for the supercritical conditions of the CO_2 at 31.26 ºC and 7.29 MPa. The high-pressure condition is not only difficult to sustain for large scale productions, but can also be dangerous.[35] Hence, ambient drying of SiO_2 aerogel is preferred, however, the process requires the microstructure of the aerogel to withstand the capillary forces of the solvent, which can be solved by a modification of the surface with an alkyl group. The method used can either be a substitution of the reagents with their carboxyl companions[36] or by carrying out a post-synthesis modification.[38-39] However, the 18-atom long carbon chain of octadecylphosphonic (ODP) used by Ref. 38, 39 for the surface modification produces narrowed pores that can significantly limit the infiltration of PCMs.

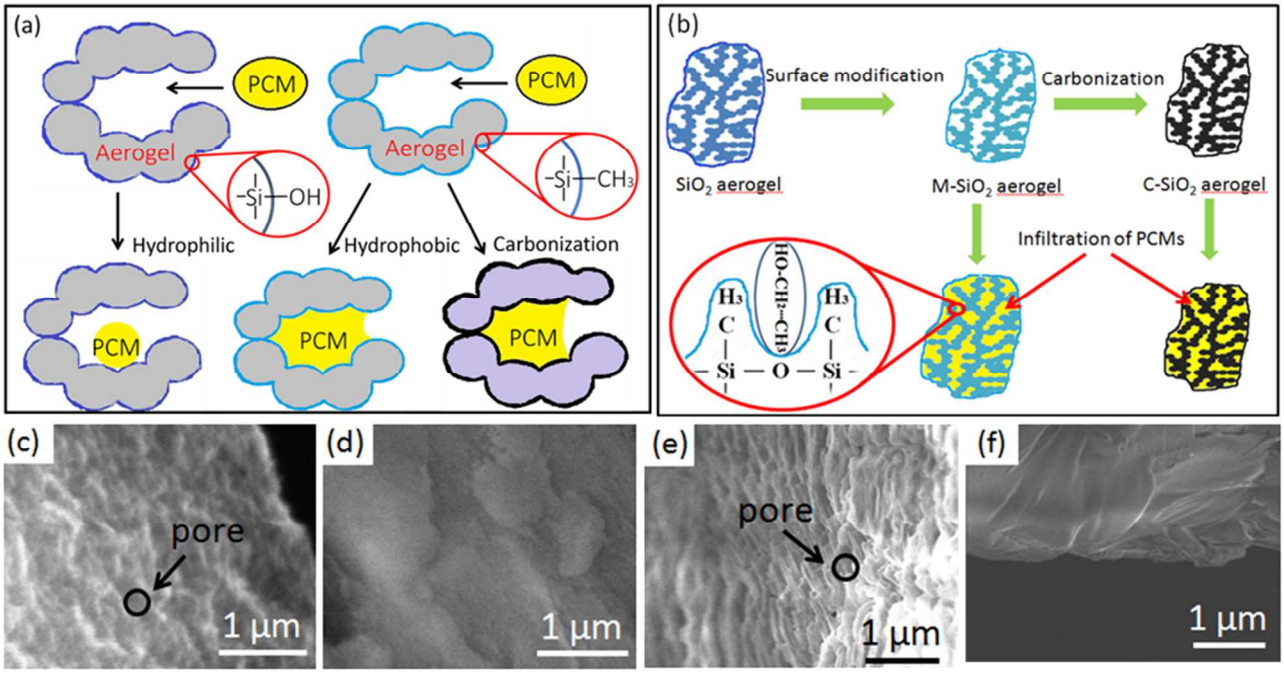

Fig. 1 Fabrication of PCM-impregnated phase change composites. (a) Schematic comparison of the PCM penetration in the untreated and treated aerogels, (b) Illustration of hydrophilic-to-hydrophobic surface modification and carbonization process. SEM images of the microstructure: (c) M-SiO_2, (d) M-SiO_2-PA, (e) C-SiO_2 and (f) C-SiO_2-OD composites. The non-infiltrated aerogels have smooth surfaces and flocculent edges, which are typical of untreated aerogels (c and e) and after infiltration the surfaces become rough with pores filled with the PCM (d and f).

In our work, we performed a surface modification with an alkyl end group on the SiO_2 aerogel by replacing Si-OH with Si-CH_3 (Fig. 1a)[40-41] using hexamethyl disilazane (HMDZ). The surface modification agent employed does not narrow the pores as much as the ODP. Further, the microstructure of the modified scaffold can withstand the capillary forces of the solvent for an ambient drying of the aerogel. We also carbonized the scaffold for a better solar heat absorption to obtain enhanced thermal energy storage and release response in the infiltrated PCM.

Compared with traditional hydrophilic SiO_2 aerogels, our surface modified hydrophobic aerogels exhibit an excellent affinity with organic hydrophobic PCMs such as the palmitic acid (PA) and the octadecanol (OD), resulting in an increased infiltration of the PCM into their mesopores (Fig. 1a). We also carbonized the treated aerogels to yield a hydrophobic scaffold with a blackened surface to better absorb the solar energy and generate sufficiently high temperatures for the phase transition in the PCM to occur. This way, the latent heat of the PCM can be used to significantly improve the thermal energy storage and release response to optimize the solar energy usage allocation.

The SiO_2 alcogels are prepared by the sol-gel method[42] involving TEOS, EtOH and oxalic acid solvent followed by hydrolysis for 12 h, dispersed in ammonia water, aged at 50 ºC for 24 h and then, dried under supercritical conditions of carbon dioxide to produce the hydrophilic SiO_2 aerogels (details in ESI†) as shown in Fig. 1b. To make the aerogels hydrophobic the alcogels are immersed in n-hexane to exchange with the ethanol. Then, the gel is immersed in HMDZ for 48 h to make the silica alcogel hydrophobic. Finally, the product is washed by n-hexane and dried at 80 ºC for 2 h to yield surface-modified silica aerogels (M-SiO_2 aerogels) in Fig. 1b, 1c. The hydrophobicity of the alkylated aerogels can be demonstrated by a simple experiment of dropping both types of aerogel into a cup of water (Fig. S1 in ESI†). The hydrophobic aerogel is seen to float on water for days, whereas, the hydrophilic aerogel rapidly absorbs water and quickly falls to the bottom in only a matter of few minutes.

We employed the vacuum method to impregnate the SiO_2 and M-SiO_2 aerogels with PA and OD separately in sealed containers (details in ESI† and Fig. 1d). [43, 44] We also carbonized some of M-SiO_2 aerogels at 900 ºC for 5 h under an Ar protective atmosphere and then, separately impregnate with PA and OD (Fig. 1b, e). Three sets of phase change composite (PCC) are fabricated: a control set consisting of a pair of untreated-PCM impregnated scaffold (SiO_2-PA, SiO_2-OD); a pair of surface modified-PCM impregnated scaffold (M-SiO_2-PA, M-SiO_2-OD); and a pair of surface modified, carbonized PCM- impregnated scaffold (C-SiO_2-PA, C-SiO_2-OD).

The pore-size distribution is ascertained using a nitrogen gas adsorption method carried out using a Quantachrome Autosorb-iQ gas adsorption analyzer. The SiO_2 aerogel is treated at 80 ºC for 5 hours and the M-SiO_2 aerogel at 200 ºC for 5 hours under vacuum with a heating rate of 10 ºC/min before gas adsorption. The N_2 adsorption and desorption isotherms were collected at 77 K in a liquid nitrogen bath (Fig. 2a). The pore size distribution of the samples is calculated by the density functional theory (DFT) using 21 partial pressure points for both adsorption and desorption isotherms (details in ESI†) and in Fig. 2b. As shown in Fig. 2b-c, the surface area of the untreated hydrophilic aerogel is comparable to the data for supercritically dried SiO_2 aerogels[45]. Also, the surface-modified hydrophobic (M-SiO_2) aerogel possesses comparable surface area and pore volume as untreated aerogel.[46] Further, the 2 treated aerogels; M-SiO_2 and C-SiO_2 possess reasonable surface area and pore volume data.[47] For control experiments, we note that the treated and untreated aerogels have comparable pore size distributions.

To demonstrate the crystalline nature of the PCCs, XRD patterns of PCM-impregnated and non-impregnated aerogels are shown in Fig. 3a-c. All 3 non-infiltrated aerogels (M-SiO_2, C-SiO_2 and SiO_2) are amorphous (Fig. 3a), whereas, the PA and OD possess good crystalline states (Fig. 3b-3c). Despite the dilution of the crystallinity

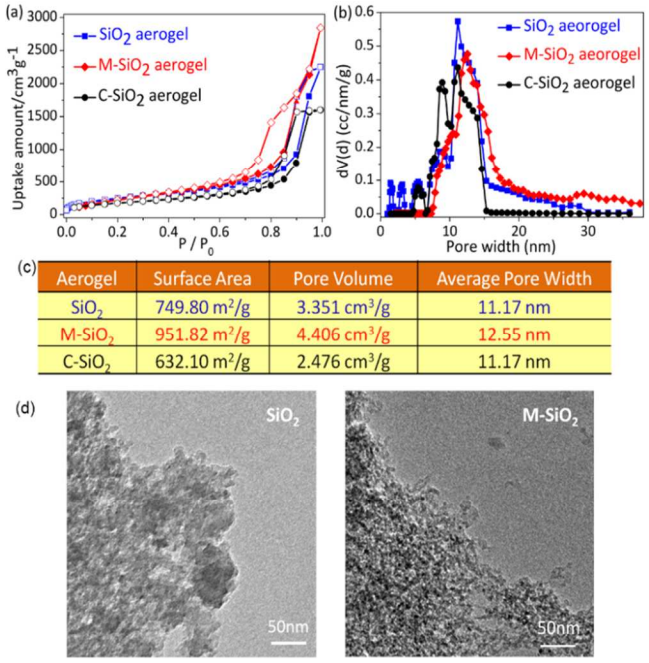

Aerogel	Surface Area	Pore Volume	Average Pore Width
SiO_2	749.80 m^2/g	3.351 cm^3/g	11.17 nm
M-SiO_2	951.82 m^2/g	4.406 cm^3/g	12.55 nm
C-SiO_2	632.10 m^2/g	2.476 cm^3/g	11.17 nm

Fig. 2 Pore structure characterization of untreated and treated aerogels. (a) Nitrogen absorption-desorption isotherms (adsorption-solid circle symbol, desorption-open circle symbol); (b) Pore size distribution; (c) Comparison of micropore structure properties of the untreated and treated aerogels; and (d) TEM images of the aerogel before and after surface-modification.

by the amorphous aerogel, the level of crystallinity in the PCCs remains high. It is also clear from the XRD patterns that the crystallinity of the SiO_2 PCC is lower than either the M-SiO_2 or C-SiO_2 PCC, and this confirms that the penetration of PCM in the hydrophilic composite is less than that of the hydrophobic composite. The data also showed that the aerogel and the PCM combined in a physical way without any chemical reaction taking place. Fig. 3d-f depicts the Fourier transform infrared (FTIR) spectra of non-infiltrated and PCM-infiltrated aerogels. We can see from the spectrum of SiO_2 aerogels that the absorption bands near 3430 cm^{-1}, 1640 cm^{-1}, and 960 cm^{-1} generated by the asymmetric stretching vibration of the –OH bond, the bending vibration of the functional group of H-OH group and the stretching vibration of the functional group of Si-OH, respectively; whereas, the bands near 1082 cm^{-1}, 796 cm^{-1} and 461 cm^{-1} are due to the asymmetric stretching, stretching vibration and bending vibration of the functional group of Si-O-Si. However, there are no signals for the functional group of Si-OH in the M-SiO_2 aerogel; instead the band near 2966 cm^{-1} is assigned to the stretching vibration of the functional group of C-H, and bands near 1259 cm^{-1}, and 848 cm^{-1} are related to the functional group of Si-C. These differences indicate that the surface-modified SiO_2 aerogel possess the hydrophobic property for the enhanced absorption of the PCM. This situation is similarly observed for the C-SiO_2 aerogel. Looking at the FTIR spectra for the composites in Fig. 3e-f, all 3 PCCs exhibit characteristic peaks of the PCMs, together with obvious absorption bands of the chemical bonds of the aerogels. Further, all the composites display distinct structures as determined by their substrates. The observed FTIR spectra are consistent with the XRD patterns in that the aerogels and either the PA or OD combine physically without the formation of a new substance in the composites.

The differential scanning calorimeter (DSC) curves (Fig. 4a, b) describe the phase change behavior of the PCM-impregnated aerogel scaffolds. As depicted, the phase change temperatures closely mirror that of the pure PCM (Fig. S2 in ESI†), which indicates that the PCM retains its thermal property after impregnation in the scaffold. This implies that the PCM undergoes a phase change at the designed temperatures as it melts and solidifies during the light-to-thermal energy experiments.

The thermal stability of our aerogel composites is characterized via a thermogravimetric (TG) analysis (Fig. 4c-f). We first consider the weight loss characteristics of the scaffold without any PCM

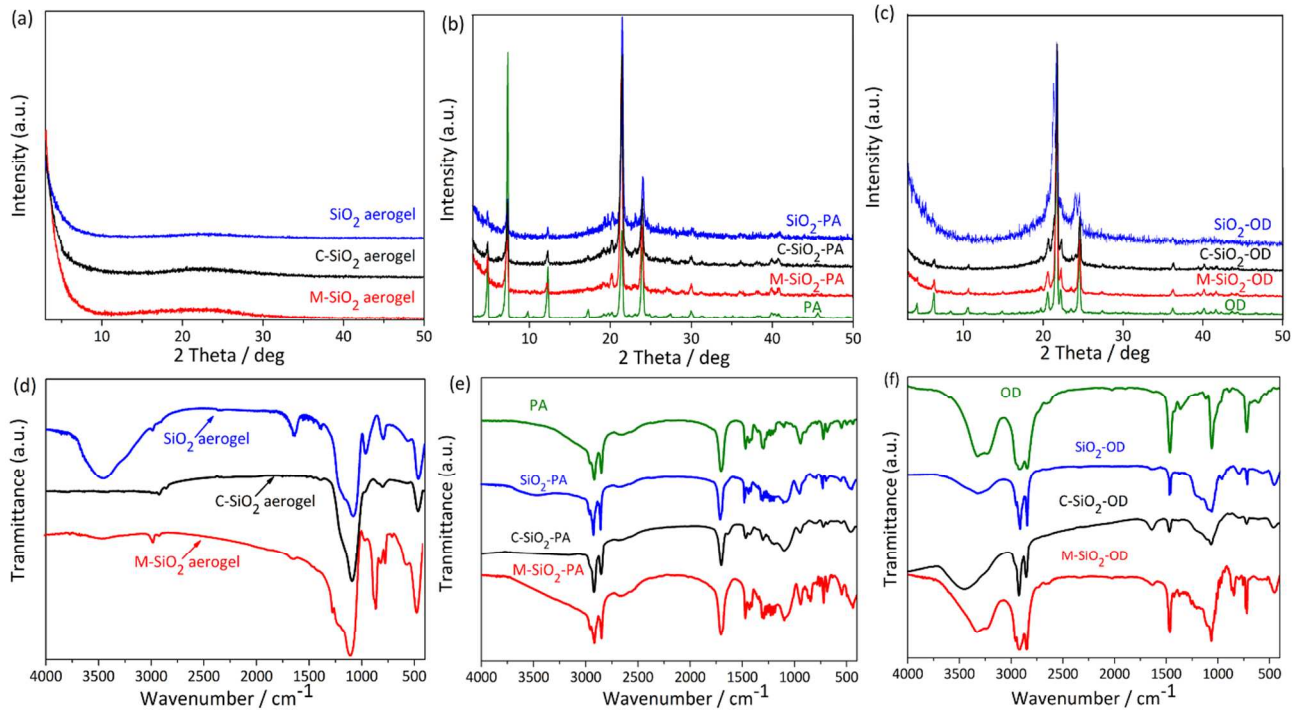

Fig. 3 XRD patterns of (a) non-impregnated aerogels; (b) PA and PA-impregnated composites; and (c) OD and OD-impregnated composites. FTIR spectra of (d) non-infiltrated aerogels; (e) PA and PA-infiltrated composites; and (f) OD and OD-infiltrated composites.

impregnation. As shown in Fig. 4c, d, both treated M-SiO_2 and C-SiO_2 aerogels exhibited very low weight loss of under 7% at temperatures up to 400 ºC. In particular, the non-infiltrated C-SiO_2 aerogel showed a remarkably low weight loss of only 3.7% at 400 ºC. On the other hand, the untreated SiO_2 aerogel experienced a large weight loss of around 16.8% at 400 ºC and this is primarily due to the loss of adsorbed water in the hydrophilic scaffold. Therefore, the surface-modified aerogel scaffolds have good thermal stability at high temperatures.

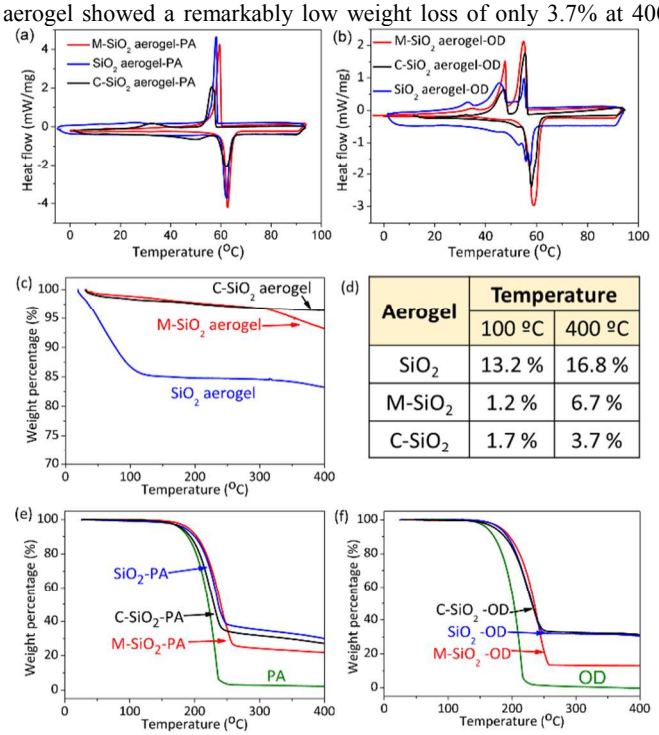

Aerogel	Temperature	
	100 ºC	400 ºC
SiO_2	13.2 %	16.8 %
M-SiO_2	1.2 %	6.7 %
C-SiO_2	1.7 %	3.7 %

Fig. 4 Thermal properties of phase change composites. (a) DSC curves for PA-infiltrated composites; (b) DSC curves for OD-infiltrated composites; (c-d) TG data for non-infiltrated aerogels; (e) TG curves for PA-infiltrated composites; (f) TG curves for OD-infiltrated

To understand the thermal stability of PCM-impregnated composites, we first studied the thermal characteristics of the pure PA and pure OD. From Fig. 4e, f it is clear that pure PA and pure OD experienced a total weight loss at between 210-230 ºC. Thus, PCM-impregnated composites exhibit a higher weight loss and at lower temperatures than the non-infiltrated aerogels. This occurs because a substantial portion of the weight loss is due to the combustion of the organic PCMs.

Table 1: Melting Enthalpy (ΔH), Infiltration Ratio (η) and Mass Ratio (M)

Sample	ΔH (kJ/kg)	$\eta = \frac{\Delta H_{PCC}}{\Delta H_{PCM}}$ %	$M = \frac{M_{bef}}{M_{aft}}$ %	$\frac{\eta}{M}$ %	Normalized ΔH (ΔH/ M %)
PA	203	100	100	1	203
OD	235	100	100	1	235
SiO_2-PA	115.27	56.8	64.2	0.885	169.76
SiO_2-OD	106.63	45.4	67.9	0.669	157.04
M-SiO_2-PA	144.36	71.1	73.5	0.967	196.41
M-SiO_2-OD	153.71	65.4	86.4	0.757	177.91
C-SiO_2-PA	104.14	51.3	61.2	0.838	170.16
C-SiO_2-OD	135.60	57.7	66.1	0.873	205.14

The phase change enthalpy can be calculated based on the enclosed area of the DSC curve during the phase change process. The results are summarized in Table 1. From the relative enthalpies of the composites versus the pure PCM, we can estimate the energy storage capacity of the composite. Hence, in Table 1, we can see that the M-SiO_2 composite possesses the highest thermal energy capacity compared to the other 2 composites.

The infiltration and mass ratios are also listed in Table 1. Together, they provide an accurate measure of the PCM penetration in the aerogel scaffold. We compared the PCM penetration in the untreated and treated (SiO_2 vs. M-SiO_2) aerogels. The average increase in the PCM uptake ranges from 20.9-34.7% with an improved thermal stability (Fig. 4c, d). Also, it would not make sense to compare the PCM penetration between the untreated and carbonized treated (SiO_2 vs. C-SiO_2) aerogels as the micropore structure of the latter would always be smaller due to the 900 ºC heating during the carbonization process. Thus, the data in Table 1 supports this expected result of a reduced PCM penetration in the carbonized treated aerogel.

The degree of PCM impregnation is one metric of performance measurement. The other is whether the PCC is able to attain the phase change temperatures of the PCM when subjected to solar irradiation in order to optimize its solar energy storage and release. To assess this aspect of the performance we carried out the light-to-thermal energy conversion experiments on the PCC (Fig. 5).

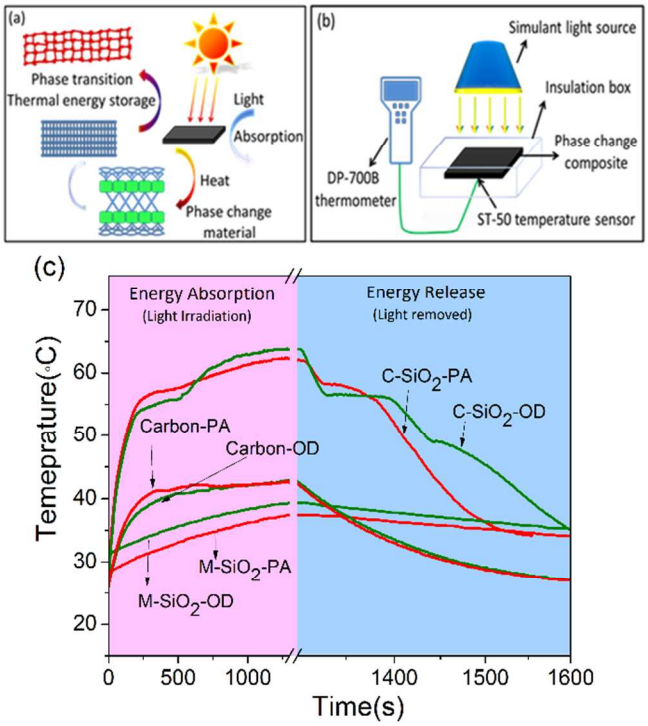

Fig. 5 Thermal energy storage and release. (a) Mechanism of light-to-heat conversion including light absorption by the carbonized phase change compact blocks and thermal energy storage by phase transition. (b) Experimental setup for light-to-heat conversion including a stimulant light source, a temperature sensor attached to the phase change composite, and a thermometer for data collection. (c) Temperature evolution curves of the PCM-impregnated compact block, carbonized PCM-impregnated compact block and PCM-embedded carbon compact block.

To prepare the samples, we pulverized the PCM-impregnated PCC in an agate mortar and compressed into a 2.5×1×0.3 cm^3 block by a steel mold. Two sets of PCC block are fabricated: treated-PCM impregnated (M-SiO_2-PCM) compact and carbonized treated-PCM impregnated (C-SiO_2-PCM) compact. The latter is coated black to capture sunlight for solar energy storage in the PCM (Fig. 5a).

Further, we fabricated a block of PCM-embedded carbon black, to provide an additional performance comparison with the 2 previous samples. Two carbon blocks, one embedded with a 61%-PA and another with 73%-OD content are synthesized – these percentages are comparable to the 2 carbonized PCM-impregnated blocks. All 3 types of compact blocks are tested in the light-to-heat conversion experiment that uses a solar simulator to irradiate the compact blocks and the temperature change is recorded in real time with a thermal sensor. (Fig. 5b).

Under a solar illumination (AM 1.5) for 1330 s duration and at an intensity of 100 mW/cm^2, only the carbonized PCM-impregnated compact block attained temperatures of above 60 ºC, which surpassed the melting temperature of the PCM (as confirmed by the DSC curves of the pure PCM in Fig. S2 in ESI†). Hence, in Fig 5c, the curves for the carbonized PCM-impregnated increase very slowly as the PCM undergoes a melting change. When the illumination is shut-off, the temperatures of the block begin to decrease from the peaked enthalpy state and as they do so, the curves exhibit several inflections as the PCM solidifies. After the phase change process is completed, the curves resume their rapid downward trend. On the other hand, under the same illumination conditions the PCM-embedded carbon block was able to reach about 43ºC, which is considerably below the phase transition temperature of the PCM. Thus, the PCM-embedded carbon block is not able to store and release energy via a phase change in the embedded PCM. In addition, we irradiated the un-carbonized PCM-impregnated block under the same conditions and the highest temperature attained is < 40 ºC. Therefore, of the 3 types of compact block tested, the carbonized PCM-impregnated compacts exhibit superior energy storage and release performance as expected.

Another issue investigated was the leakage of the PCM – to see if the compacted blocks were able to hold on to the impregnated PCM. We heated the pure PCM and PCM-impregnated compact blocks in a hot plate a target temperature set a little higher than the melting point of the PCM. As shown in Fig. S6 (in ESI†) after heating for T=150 s the pure PCM block melted away like a slurry whereas, the PCM-impregnated block remained essentially intact without any PCM leakage. It is clear that grinding and compacting actions during the sample preparation did not weaken the form-stable property of the composite compact block.

Conclusions

We surface modified the hydrophilic silica aerogels at ambient pressures to make them hydrophobic for an effective PA or OD impregnation. The increased PCM uptake is observed to be in the range of 20.9-34.7% with an improved thermal energy storage capacity and stability. Also, we fabricated carbonized PCM-impregnated and PCM-embedded carbon compact blocks and used them for the light-to-thermal energy conversion experiments. We showed that only the carbonized PCM-impregnated block exhibits superior solar energy storage and release response.

Acknowledgement

We appreciate the funding support from the National Natural Science Foundation of China (Grant No. 51322205 and 21371014), the National Basic Research Program of China (Grant No. 2009CB939902), New Star Program of Beijing Committee of Science and Technology (Grant No. 2012004), and the Ministry of Education Program for New Century Excellent Talents of China (Grant No. NCET-11-0027).

Notes and references

Peking University, Department of Materials Science and Engineering, College of Engineering, Beijing, China 100871.
‡These authors contribute equally.
*Email: R. Han (ray-han@pku.edu.cn) and R. Zou (rzou@pku.edu.cn).
†Electronic Supplementary Information (ESI) available: [for the synthesis of silica aerogels and phase change materials; and their characterizations]. See DOI: 10.1039/c000000x/

1 R. Shinnar, *Science*, 2005, **310**, 620.
2 S. Chu and A. Majumdar, *Nature*, 2012, **488**, 294-303.
3 Y. Wang, B. Tang and S. Zhang, *J. Mater. Chem.*, 2012, **22**, 18145-18150.
4 S. Hasnain, *Energ. Convers. Manag.*, 1998, **39**, 1127-1138.
5 C. Wu, W. Xie, M. Zhang, L. Bai, J. Yang and Y. Xie, *Chem.-Eur. J.*, 2009, **15**, 492-500.
6 J. Zhang, S. Wang, S. Zhang, Q. Tao, L. Pan, Z. Wang, Z. Zhang, Y. Lei, S. Yang and H. Zhao, *J. Phys. Chem. C*, 2011, **115**, 20061-20066.
7 C. Wu, X. Zhang, B. Ning, J. Yang and Y. Xie, *Inorg. Chem.*, 2009, **48**, 6044-6054.
8 B. Zalba, J. M. Marín, L. F. Cabeza and H. Mehling, *Appl. Therm. Eng.*, 2003, **23**, 251-283.
9 A. M. Khudhair and M. M. Farid, *Energ. Convers. Manag.*, 2004, **45**, 263-275.
10 M. M. Farid, A. M. Khudhair, S. A. K. Razack and S. Al-Hallaj, *Energ. Convers. Manag.*, 2004, **45**, 1597-1615.
11 L. Pan, Q. Tao, S. Zhang, S. Wang, J. Zhang, S. Wang, Z. Wang and Z. Zhang, *Sol. Energ. Mater. Sol. C.*, 2012, **98**, 66-70.
12 H. Babaei, P. Keblinski and J. Khodadadi, *Int. J. Heat. Mass. Tran.*, 2013, **58**, 209-216.
13 H. Babaei, P. Keblinski and J. Khodadadi, *Phys. Lett. A*, 2013, **377**, 1358-1361.
14 A. Sharma, V. V. Tyagi, C. R. Chen and D. Buddhi, *Renew. Sust. Energ. Rev.*, 2009, **13**, 318-345.
15 F. Yavari, H. R. Fard, K. Pashayi, M. A. Rafiee, A. Zamiri, Z. Yu, R. Ozisik, T. Borca-Tasciuc and N. Koratkar, *J. Phys. Chem. C*, 2011, **115**, 8753-8758.
16 A. Mallow, O. Abdelaziz, K. Kalaitzidou and S. Graham, *J. Mater. Chem.*, 2012, **22**, 24469-24476.
17 S. Zhang, Q. Tao, Z. Wang and Z. Zhang, *J. Mater. Chem.*, 2012, **22**, 20166-20169.
18 A. Sari and K. Kaygusuz, *Sol. Energy*, 2001, **71**, 365-376.
19 A. F. Regin, S. C. Solanki and J. S. Saini, *Renew. Sust. Energ. Rev.*, 2008, **12**, 2438-2458.
20 S. Phadungphatthanakoon, S. Poompradub and S. P. Wanichwecharungruang, *ACS Appl. Mater. Interfaces*, 2011, **3**, 3691-3696.
21 Y. Hong, S. Ding, W. Wu, J. Hu, A. A. Voevodin, L. Gschwender, E. Snyder, L. Chow and M. Su, *ACS Appl. Mater. Interfaces*, 2010, **2**, 1685-1691.
22 L. Pan, Q. Ji, Y. Qin, Y. Jiang, Z. Zhang, S. Zhang and Z. Wang, *RSC Adv.*, 2013, **3**, 22326-22331.
23 S. Zhang, S. Wang, J. Zhang, Y. Jiang, Q. Ji, Z. Zhang and Z. Wang, *J. Phys. Chem. C*, 2013, **117**, 23412-23417.
24 W. Wang, C. Wang, W. Li, X. Fan, Z. Wu, J. Zheng and X. Li, *Phys. Chem. Chem. Phys.*, 2013, **15**, 14390-14395.
25 Z. Liu, R. Zou, Z. Lin, X. Gui, R. Chen, J. Lin, Y. Shang and A. Cao, *Nano Lett.*, 2013, **13**, 4028-4035.
26 C. Wang, L. Feng, W. Li, J. Zheng, W. Tian and X. Li, *Sol. Energ. Mater. Sol. C.*, 2012, **105**, 21-26.
27 L. Feng, J. Zheng, H. Yang, Y. Guo, W. Li and X. Li, *Sol. Energ. Mater. Sol. C.*, 2011, **95**, 644-650.
28 L. Feng, W. Zhao, J. Zheng, S. Frisco, P. Song and X. Li, *Sol. Energ. Mater. Sol. C.*, 2011, **95**, 3550-3556.
29 L. Chen, R. Zou, W. Xia, Z. Liu, Y. Shang, J. Zhu, Y. Wang, J. Lin, D. Xia and A. Cao, *ACS Nano*, 2012, **6**, 10884-10892.

30 J. Fricke and T. Tillotson, *Thin Solid Films*, 1997, **297**, 212-223.
31 D. W. Schaefer and K. D. Keefer, *Phys. Rev. Lett.*, 1986, **56**, 2199-2202.
32 H. Gesser and P. Goswami, *Chem. Rev.*, 1989, **89**, 765-788.
33 H. Sun, Z. Xu and C. Gao, *Adv. Mater.*, 2013, **25**, 2554-2560.
34 X. Zhou, H. Xiao, J. Feng, C. Zhang and Y. Jiang, *J. Exp. Nanosci.*, 2012, **7**, 17-26.
35 J. L. Gurav, I. K. Jung, H. H. Park, E. S. Kang and D. Y. Nadargi, *J. Nanomater.*, 2010.
36 F. Shi, L. J. Wang and J. X. Liu, *Mater Lett*, 2006, **60**, 3718-3722.
37 P. M. Shewale, A. V. Rao, A. P. Rao and S. D. Bhagat, *J Sol-gel Sci Techn*, 2009, **49**, 285-292.
38 D. Ebert and B. Bhushan, *Langmuir*, 2012, **28**, 11391-11399.
39 Y. Zhou, S.-T. Han, Z.-X. Xu, X.-B. Yang, H.-P. Ng, L.-B. Huang and V. A. L. Roy, *J Mater Chem*, 2012, **22**, 14246-14253.
40 H. Yokogawa and M. Yokoyama, *J. Non-Cryst. Solids*, 1995, **186**, 23-29.
41 A. P. Rao and A. V. Rao, *J. Mater. Sci.*, 2010, **45**, 51-63.
42 J. L. Gurav, D. Y. Nadargi and A. V. Rao, *Appl. Surf. Sci.*, 2008, **255**, 3019-3027.
43 D. Zhang, J. Zhou, K. Wu and Z. Li, *Sol. Energy*, 2005, **78**, 471-480.
44 D. Zhang, S. Tian and D. Xiao, *Sol. Energy*, 2007, **81**, 653-660.
45 A. C. Pierre and G. M. Pajonk, *Chemical Reviews* 2002, **102**, 4243–4265. doi:10.1021/cr0101306.
46 R. Maloney and J. Sakamoto, *Non-Crystalline Solids*, 2011, **35**, 2059-2062.
47 P. B. Sarawade, J.-K. Kim, H.-K. Kim and H.-T. Kim, *Appl Surf Sci*, 2007, **254**, 574-579.

